Biosensors and Bioelectronics 132 (2019) 265–270

Contents lists available at ScienceDirect

Biosensors and Bioelectronics

journal homepage: www.elsevier.com/locate/bios

"Off-on" signal amplification strategy amperometric immunosensor for ultrasensitive detection of tumour marker

Huiqiang Wang [a,b,c], Zhanfang Ma[a,*]

[a] Department of Chemistry, Capital Normal University, Beijing 100048, China
[b] Beijing National Laboratory for Molecular Sciences (BNLMS), Key Laboratory of Green Printing, Institute of Chemistry, Chinese Academy of Sciences, Zhongguancun North First Street 2, Beijing 100190, China
[c] University of Chinese Academy of Sciences, Beijing 100049, China

ARTICLE INFO

Keywords:
Sensitivity
Hydroquinone
Amperometric immunosensor
Tumour marker
ZIF-8
Cytokeratins antigen 21-1

ABSTRACT

Reducing background signal is an effective method to improve the sensitivity of amperometric immunosensors, which are significant in the detection of cancer. Herein, a novel immunosensor probe was synthesised using zeolitic imidazolate framework-hydroquinone-bovine serum albumin (ZIF-8-HQ-BSA). Based on the probe, an "off-on" strategy was applied in the immunosensor to amplify ΔI, the current signal "turn off and on". The ZIF-8-HQ-BSA probe initially showed little current signal since ZIF-8 and BSA exhibit poor conductivity. To amplify the current signal "turn on", the structure of ZIF-8 was broken after treatment with HCl, releasing hydroquinone to be absorbed by the polyaniline hydrogel substrate. Hydroquinone can produce a strong signal and also exhibits strong catalytic ability for H_2O_2 to further enhance the signal. Following this method, the immunosensing platform was used to detect cytokeratins antigen 21-1 (CYFRA21-1) in human serum and revealed a wide liner range from 0.1 pg mL^{-1} to 100 ng mL^{-1} with a low detection limit of 0.65 pg mL^{-1} (S/N = 3), demonstrating good consistency with an electrochemiluminescence immunoassay. Thus, the amperometric immunosensing platform discussed in this work has high potential for application in healthcare monitoring, clinical diagnostics, and biomedical devices.

1. Introduction

Cancer is a leading cause of health decline in humans with the number of deaths increasing each year. Early detection is the key to enhance successful treatment of the disease, leading to increased patient survival rate (Danielle et al., 2012; Wang et al., 2006, 2017; Wang and Ma, 2017; Tang et al., 2017a, 2017b). A tumour marker is a substance that a tumour cell has produced or produces during the development and growth of cancer (Wang et al., 2017; Tang et al., 2017a, 2017b). Therefore, the determination of tumour markers plays an important role in the early detection of cancers. Recently, great efforts have been made to the detect tumour biomarker, such as enzyme-linked immunosorbent assay (ELISA), fluorescence immunoassay, chemiluminescence assay, radio immunoassay, and electrochemiluminescence assay (Tang et al., 2017a, 2017b; Shan et al., 2016; Wang et al., 2014a, 2014b; Zou et al., 2017; Wang et al., 2011, 2003). Although each of these methods has shown effective detection, there are also some inevitable drawbacks, including: (1) the preparation time of ELISA is time-consuming; (2) the chemiluminescence assay has poor selectivity; (3) and fluorescence immunoassay fluorescence immunoassay has exhibited signal instability and high background signal. Thus, the development of a highly sensitive and efficient immunoassay is largely desirable for tumour marker detection.

Electrochemical immunoassays have shown to be a reliable, time-saving method with good sensitivity, which is an important indicator of detection efficiency (Tang et al., 2017a, 2017b). Currently, several common methods are available to increase sensitivity. (1) Catalytic nanomaterials, such as noble metal nanoparticles and biological enzymes, are often used to catalyse signal amplification. However, noble metals and biological enzymes are expensive, and the application condition of enzymes requires a tedious procedure. These disadvantages limit their application in clinical diagnosis to some extent (Fan et al., 2015; Liu et al., 2013, 2014; Sanati et al., 2014). (2) Conductive substrates composed of noble metals and carbon materials, which exhibit good conductivity and a large specific surface area, can produce a large electrochemical signal and improve sensitivity. Yet, carbon nanotubes require strict conditions for the activation process using strong acid heating reflux, and graphene has poor solubility and a

* Corresponding author.
E-mail address: mazhanfang@cnu.edu.cn (Z. Ma).

https://doi.org/10.1016/j.bios.2019.03.013
Received 16 December 2018; Received in revised form 7 March 2019; Accepted 8 March 2019
Available online 09 March 2019
0956-5663/

tedious post processing (Karimi-Maleh et al., 2013; Liu et al., 2014; Moradi et al., 2013; Sanati et al., 2014; Tang et al., 2016; Liang et al., 2017). (3) Redox nanomaterials, including redox metal ions, redox inorganic nanocrystals, and organic dye molecules, are used in amperometric immunoassays, in which the electrochemical activity and quantity of redox species can significantly affect the strength of the current signal. To receive powerful signals, these redox materials generally possess some advantageous properties in terms of the amount of redox sites, large specific area, good hydrophilicity, conductivity, low-cost, and easy acquirement (Wang et al., 2006, 2014a, 2014b; Wilson, 2005; Xia et al., 2010; Yang et al., 2014). Given the above disadvantages, it is of great significance to develop new redox materials and a strategy for fabricating an ultrasensitive electrochemical immunosensor.

Zeolitic imidazolate framework-8 (ZIF-8), a new kind of MOF, exhibit numerous advantages, including large surface areas, uniform pore structure, high porosity, and low density, which can load and release different substances (Cheng et al., 2016; Lyu et al., 2014; Zheng et al., 2016). However, most MOFs are insulators, limiting the application of ZIF-8 in biosensors. Furthermore, ZIF-8 shows chemical stability in water but is immediately broken down in acidic solutions due to its pH-sensitive properties, making it an appealing candidate for use in electrochemical immunosensor.

Herein, a novel ZIF-8-HQ-BSA probe was synthesised by the self-assembly of Zn^{2+}, imidazolate, hydroquinone, and BSA. ZIF-8 can absorb hydroquinone and BSA through electrostatic interaction to prepare a ZIF-8-HQ-BSA probe. The “off-on” strategy based on this probe can be implemented in the immunosensor to amplify ΔI, which can effectively reduce the background signal. Initially, the ZIF-8-HQ-BSA probe demonstrated a small current signal due to the poor conductivity of ZIF-8 and BSA. After treatment with HCl, the structure of ZIF-8 was broken, releasing hydroquinone, which was then absorbed by the polyaniline hydrogel substrate. Hydroquinone produced a strong signal at about 0.1 V (vs Ag/AgCl) and exhibited strong catalytic ability for H_2O_2 to further enhance the signal. Based on the “off-on” strategy, the proposed immunosensor presents excellent sensing performance to detect cytokeratins antigen 21-1 (CYFRA21-1) with a wide high sensitivity and wide linear range.

2. Experimental

2.1. Materials

Carcino-embryonic antigen (CEA), alpha fetoprotein (AFP), prostate specific antigen (PSA), and cytokeratins antigen 21-1 (CYFRA21-1) were obtained from Shanghai Linc-Bio Science Company. Human immunoglobulin G (IgG) was obtained from Beijing Xinjingke Biotechnology Company. Matrix metalloproteinase-7 (MMP-7) was purchased from Shanghai Yi Sheng Biotechnology Co., Ltd (Shanghai, China). HCl, glucose, uric acid (UA), and ascorbic acid (AA) were obtained from Alfa Aesar (Tianjin, China). Hydroquinone, H_2O_2 (30%), zinc nitrate, 2-methylimidazole, polishing powder, $K_3Fe(CN)_6$, $K_4Fe(CN)_6$, NaH_2PO_4, Na_2HPO_4, KCl and ethanol were achieved from Beijing Chemical Reagents Company (Beijing, China). Human serum samples were achieved from Beijing Bainuowei Company (Beijing, China). All other reagents were of analytical grade and used without any further purification. All aqueous solutions were prepared with ultrapure water (resistivity > 18 MΩ cm).

2.2. Apparatus

All apparatus were placed in Electronic Supplementary material.

2.3. Synthesis of ZIF-8-HQ-BSA

(a) Preparation of ZIF-8: ZIF-8 was synthesised according to previous literatures with slight modifications (Cheng et al., 2016; Lyu et al., 2014; Zheng et al., 2016). Two separate 50 mL solutions were prepared, one containing zinc nitrate hexahydrate in methanol (0.7436 g, 50 mM), and one with 2-methylimidazole in methanol (0.2053 g, 50 mM). The mixtures were kept at 35 °C for 24 h, and the obtained white precipitates were centrifuged at 8000 rpm for about 10 min and then washed with methanol 5 times. Ultimately, the composites were re-dispersed in 1.0 mL ultrapure water.

(b) Preparation of ZIF-8-HQ-BSA: 1.0 mL hydroquinone (0.011 g, 0.1 M) was added into the ZIF-8 solution under stirring for 3 h and absorbed into ZIF-8 by electrostatic interaction. Then, 1.0 mL BSA (0.01 g, 1 wt%) was mixed in the above solution under stirring for 2 h. The obtained white precipitates were centrifuged and washed by deionized water several times. Finally, the synthesised ZIF-8-HQ-BSA was redistributed in 1.0 mL ultrapure water.

2.4. Preparation of the immunoprobe

The immunosensing probe was fabricated by immobilising labelled anti-CYFRA21-1 onto ZIF-8-HQ-BSA nanocomposites. Subsequently, the ZIF-8-HQ-BSA composite was added into a solution containing EDC (50 mM) and NHS (50 mM), and the mixture was stirred for 12 h. Then, 1.0 mL labelled anti-CYFRA21-1 solution (1 mg mL^{-1}) was injected into the above solution. After 4 h of reaction with stirring, the mixture was centrifuged and re-dispersed into 1.0 mL PBS (pH = 7.4).

2.5. Fabrication of the proposed amperometric immunosensor

Prior to the functionalization procedure, a glassy carbon electrode (GCE) was polished with 0.05-μm alumina polishing powder, then treated with ultrapure water and ethanol three times and dried at 37 °C. The polyaniline (PANI) hydrogel film was successfully electrodeposited on the GCE under a constant potential of 0.80 V for 400 s in an aqueous solution containing aniline (0.5 M), phytic acid (0.15 M), and KCl (1 M). After being washed several times, AuNPs were deposited on the PANI film under a constant potential of −0.20 V for 30 s at a scan rate of 50 mVs^{-1} in 0.50 mM $HAuCl_4$ solution (containing 1 mM KCl). After washing, 70 μL of 200 μg mL^{-1} capture antibodies (anti-CYFRA21-1) were dropped on the PANI hydrogel/Au-modified GCE and incubated for 12 h at 4 °C to anchor the antibody to the surface of electrode. Subsequently, 20 μL BSA (1 wt%) was used to block the nonspecific active sites. After washed with purified water, the modified electrode was obtained and stored at 4 °C before use.

2.6. Electrochemical measurement

To carry out the detection process, the biosensor was first incubated with a sequence of standard solutions of CYFRA21-1 with different concentrations at 37 °C for 60 min. The biosensor was then washed with ultrapure water thoroughly. Next, 20 μL of the prepared ZIF-8-HQ-BSA-Ab_2 solution was dropped onto the electrode surface and incubated at 37 °C for 60 min and washed thoroughly with ultrapure water. Finally, a sandwich reaction was performed to detect CYRRA21-1. Square wave voltammetry (SWV) was conducted in a phosphate buffered solution with a 50 mV s^{-1} sweeping rate, 2 s quiet time, voltage range from −0.5–0.75 V, and 50 ms pulse width.

3. Results and discussion

3.1. Principle of the “off-on” strategy-based amperometric immunosensor

The fabrication procedure and detection principle of the “off-on” signal amplification strategy of the amperometric immunosensor are demonstrated in Scheme 1. Polyaniline hydrogel with a large specific surface and good conductivity was electrodeposited on the surface of GCE, which can absorb hydroquinone contained in the ZIF-8-HQ-BSA

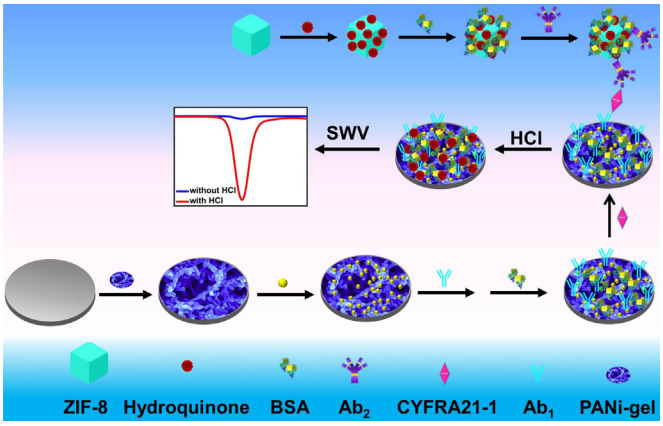

Scheme 1. Schematic illustration of the "off-on" signal amplification strategy amperometric immunosensor.

probe. AuNPs, possessing good conductivity, were electrodeposited onto the polyaniline hydrogel to immobilise the anti-CYFRA21-1. Using ZIF-8-HQ-BSA nanocomposites as an immunoprobe, an "off-on" strategy was applied in the immunosensor to amplify ΔI. Initially, the ZIF-8-HQ-BSA probe showed little current signal due to the poor conductivity of ZIF-8 and BSA. After treatment with HCl, the structure of ZIF-8 was broken, and its contained hydroquinone was released and absorbed by the substrate polyaniline hydrogel. Then, the hydroquinone produced a strong signal at about 0.1 V (vs Ag/AgCl) and exhibited strong catalytic ability for H_2O_2 to further enhance the signal (Fig. S1). Following this method, the immunosensor showed a wide liner range and high sensitivity.

3.2. Characterisation of ZIF-8, ZIF-8-HQ, and ZIF-8-HQ-BSA

The morphologies and sizes of ZIF-8, ZIF-8-HQ, and ZIF-8-HQ-BSA were characterised by TEM analysis (Fig. 1A–C). As shown in Fig. 1A, the obtained nanocubes had smooth surfaces and were uniform, with an average diameter of approximately 200 nm, which is consistent with SEM picture. Similar to pure ZIF-8, the ZIF-8-HQ composite displayed the same morphology with smooth surfaces (Fig. 1B), then after modification with BSA, the ZIF-8-HQ-BSA composite exhibited rough surfaces (Fig. 1C). Moreover, the X-ray diffraction (XRD) pattern of ZIF-8-HQ and ZIF-8-HQ-BSA composite also agrees well with that of pure ZIF-8, which indicates that the structure of ZIF-8 did not deteriorate during assembly (Fig. 1D). In order to address the adsorption of hydroquinone by ZIF-8, the process of ZIF-8 adsorbing hydroquinone was investigated by UV–Vis and zeta potential measurements (Fig. 1E). While there was no obvious absorption peak for the pure ZIF-8, an absorption peak at 252 nm appeared after the successful encapsulation of hydroquinone, corresponding to the characteristic absorption peak of hydroquinone solution. To confirm the adsorption process of hydroquinone by ZIF-8, zeta potentials of ZIF-8 and hydroquinone were initially measured to be 20 and −12 mV, respectively. After adsorption of hydroquinone, the zeta potential of ZIF-8-HQ was 3 mV, indicating that hydroquinone was successfully adsorbed by ZIF-8 (Fig. 1F).

3.3. Proof tests of the "off-on" strategy

SEM, X-ray diffraction (XRD), SWV, and zeta potential were carried out to investigate the "off-on" mechanism. The structure of ZIF-8 was broken within ten seconds through the treatment of 0.1 M HCl, and its contained hydroquinone was released and absorbed by the substrate polyaniline hydrogel. The SEM image of the anti-CYFRA21-1/AuNPs/PANI hydrogel/GCE revealed a hierarchically porous and 3D network structure (Fig. 2A). After immobilisation of the ZIF-8-HQ-BSA probe,

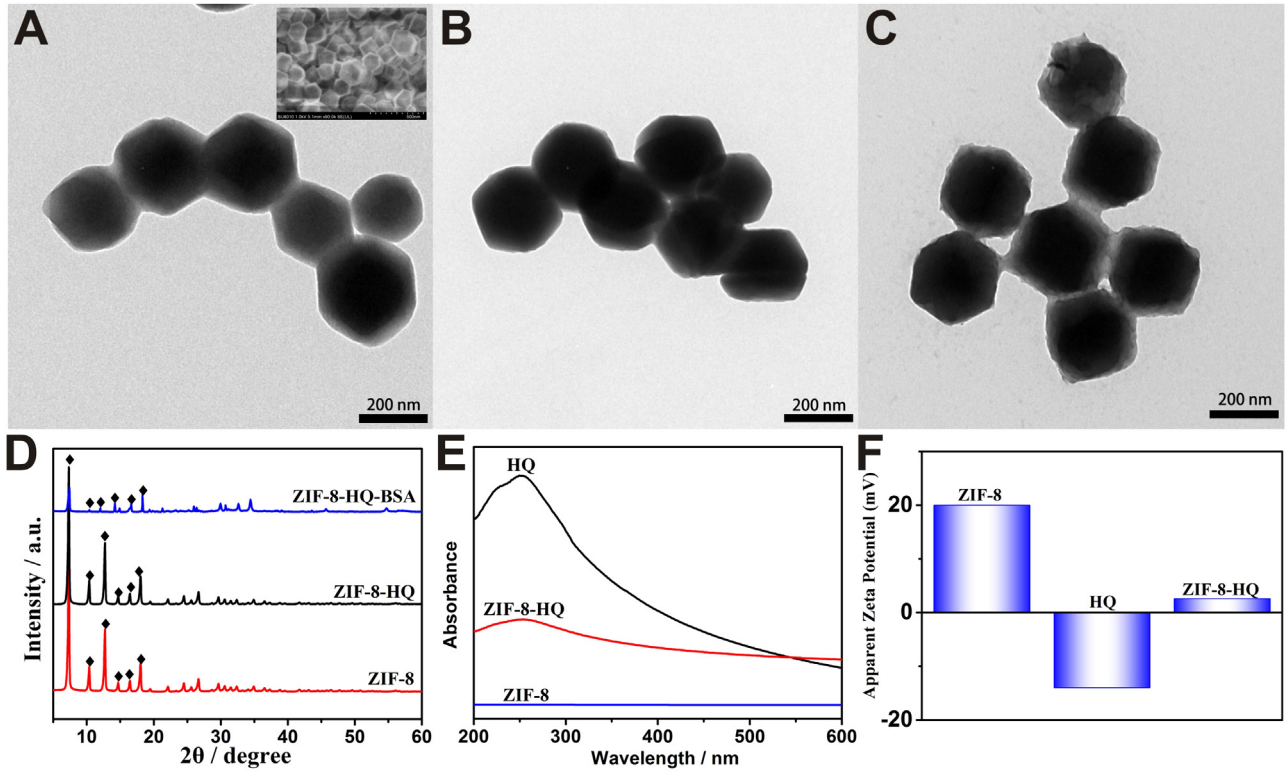

Fig. 1. Characterisation of ZIF-8-HQ-BSA nanocomposites. TEM images of ZIF-8 particles (A), ZIF-8-HQ particles (B), ZIF-8-HQ-BSA nanocomposites (C); XRD curves of ZIF-8-HQ-BSA assembly (D): pure ZIF-8, ZIF-8-HQ particles, ZIF-8-HQ-BSA nanocomposites; UV–Vis spectra of ZIF-8-HQ assembly (E): pure ZIF-8, hydroquinone, ZIF-8-HQ. Zeta potential measurements of ZIF-8-HQ assembly (F): pure ZIF-8, hydroquinone, ZIF-8-HQ.

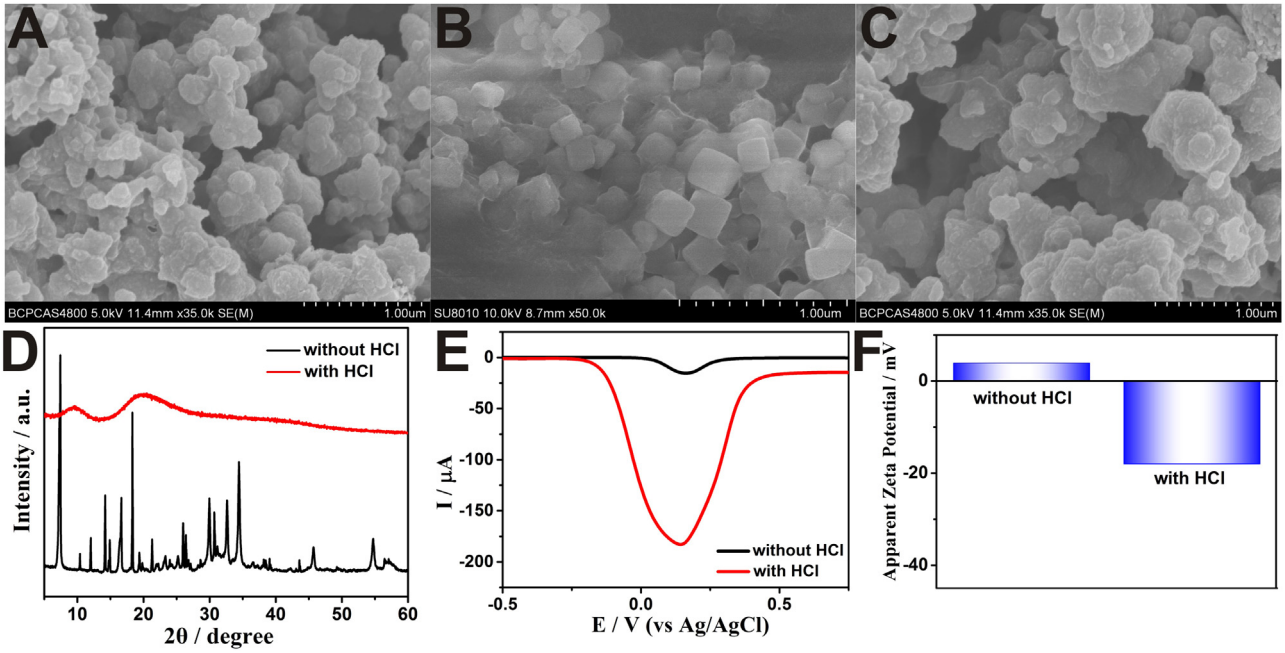

Fig. 2. Proof tests of the "off-on" strategy. SEM micrographs of anti-CYFRA21-1/AuNPs/PANI hydrogel/GCE (A), ZIF-8-HQ-BSA-Ab_2-CYFRA21-1- anti-CYFRA21-1/AuNPs/PANI hydrogel/GCE treated without (B) and with (C) hydrochloric Acid; XRD curves of ZIF-8-HQ-BSA before and after treated with hydrochloric acid (D); Amperometric curves of the immunosensor before and after treated with hydrochloric acid (E); Zeta potential measurements of ZIF-8-HQ-BSA before and after treated with hydrochloric acid (F).

cubic nanoparticles can be clearly seen (Fig. 2B), which indicates that the ZIF-8-HQ-BSA probe was successfully attached on the proposed immunosensor. The cubic nanoparticles disappeared after the HCL treatment, indicating that the structure of ZIF-8 was broken (Fig. 2C). The XRD patterns of the ZIF-8-HQ-BSA composite treated with and without HCl were different, which reveals that the structure of ZIF-8 was changed by HCL (Fig. 2D). Meanwhile, a significant signal increase was observed for the immunosensor treated with HCl (Fig. 2E). Zeta potentials of ZIF-8-HQ-BSA before and after HCL treatment were 3 and −17 mV (Fig. 2F), respectively, further confirming that the ZIF-8 structure was deteriorated by HCL. In addition, the catalytic ability of PANI-hydrogel-hydroquinone towards H_2O_2 was investigated by amperometric i-t at −0.2 V (vs Ag/AgCl) in 40 mL PBS. A high current response was obtained, indicating that hydroquinone can be oxidised by H_2O_2 to enhance the current signal (Fig. S1A). Also, the signal increased significantly when the immunosensor was treated with H_2O_2 (Fig. S1B), which suggests that hydroquinone exhibits excellent H_2O_2 catalytic ability.

3.4. Construction procedures of the modified electrodes

The stepwise modification process of the electrodes was determined using square wave voltammetry (SWV) (Fig. 3A) and electrochemical impedance spectroscopy (EIS) (Fig. 3B) in 5 mM $[Fe(CN)_6]^{3-/4-}$. In Fig. 3A, the current response of the PANI hydrogel-modified GCE (curve b) was higher than that of bare GCE (curve a), which is attributed to the good conductivity and large specific surface area of the hydrogel. When AuNPs were electrodeposited onto the surface of the hydrogel, the current response further increased (curve c), due to the following causes: (1) after AuNPs were electrodeposited onto the modified GCE, the effective surface area increased 5.37%, which can accelerate the ion transmission (Fig. S2) (the effective surface areas of the modified GCE before and after electrode-deposition of AuNPs were measured and were 23.32 and 22.13 mm^2, respectively); (2) after electro-deposition of AuNPs, the capacitance increased 6.18% (the capacitance of the modified GCE before and after electrode-deposition of AuNPs was measured and was 114.12 and 121.17 μF, respectively). Thus, after AuNPs were electrodeposited onto the surface of the hydrogel, the capacitive current has increased (Fig. S3); (3) AuNPs possessed good conductivity, which can accelerate the electron transfer (Fig. S4). In contrast, the loading of anti-CYFRA21-1 led to an obvious decrease in the peak current (curve d), owing to the formation of an electron-blocking layer. Subsequently, it was found that the current response also decreased after the immunosensor was blocked with BSA (curve e) and incubated in a solution of CYFRA21-1 (curve f). The current decrease can be attributed to the insulating layers of BSA and CYFRA21-1 proteins on the electrode, which retarded electron transfer. Finally, after immobilisation of the ZIF-8-HQ-BSA-Ab_2 immunoprobe, the current signal almost vanished (curve g).

Fig. 3B shows that the Nyquist diagrams of the sensing electrode changed gradually with the stepwise modification process. The Nyquist plots of EIS consist of two portions: the linear part and the semicircle part. The linear portion at low frequencies represents the diffusion-limited process, while the semicircle diameter at higher frequencies corresponds to the electron-transfer resistance. After the GCE was modified with the hydrogel (curve b), the diameter of the semicircle was much smaller than that of the bare GCE (curve a), revealing that the hydrogel film possesses excellent conductivity. When AuNPs were electrodeposited onto the surface of the hydrogel, the resistance response increased (curve c). Following the stepwise immobilisation of anti-CYFRA21-1, BSA, CYFRA21-1, and ZIF-8-HQ-BSA-Ab_2, the resistance increased gradually (curves d–g), since the nonconductive layer of proteins hindered electron transfer on the interface. Thus, the tendency of electron-transfer resistance in EIS plots to vary verifies the results of the SWV plots in the same modification process. Table S1 shows the specific values of SWV and EIS for the stepwise fabrication process of the immunosensor.

3.5. Optimisation of the detection conditions

To achieve the best analytical performance of the proposed immunosensor, the HQ concentration for the fabrication of ZIF-8-HQ-BSA, H_2O_2 concentration for signal amplification, incubation time, and pH were optimised by incubating with 1 ng mL^{-1} CYFRA21-1 and

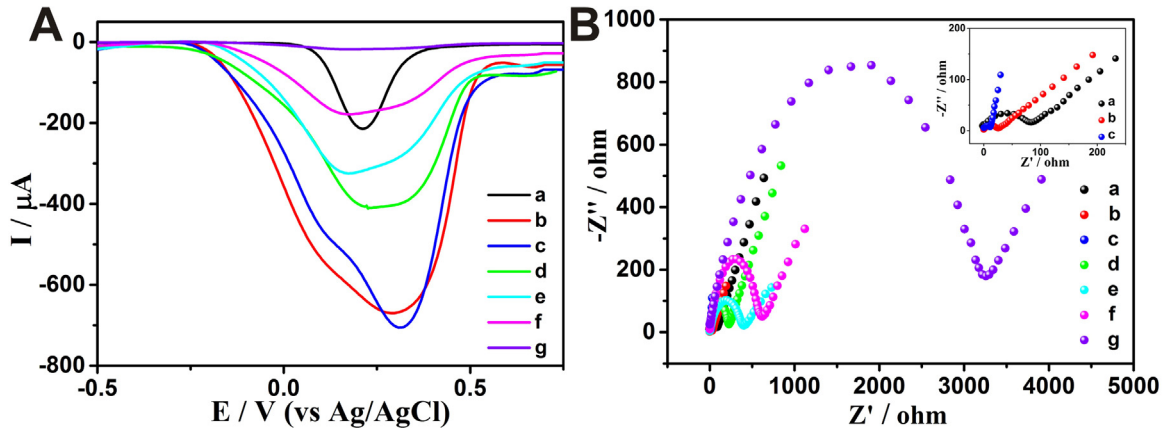

Fig. 3. SWV (A) and EIS (B) of different modified electrodes in 0.01 M phosphate buffered solution containing 5.0 mM $[Fe(CN)_6]^{4-/3-}$ and 0.1 M KCl: bare GCE (curve a), PANI hydrogel/GCE (curve b), AuNPs/PANI hydrogel /GCE (curve c), anti-CYFRA21-1/AuNPs/PANI hydrogel/GCE (curve d), the modified electrode was blocked with BSA (curve e) , CYFRA21-1-anti-CYFRA21-1/AuNPs/PANI hydrogel/GCE (curve f), ZIF-8-HQ-BSA-Ab_2-CYFRA21-1- anti-CYFRA21-1/AuNPs/PANI hydrogel/GCE (curve g).

monitoring the currents with SWV. As shown in Fig. S5A, 0.1 M hydroquinone was chosen as the optimal condition for subsequent experiments. Fig. S5B shows that the peak current increased over time and reached a steady value at 5 mM H_2O_2, so this concentration was adopted for signal amplification. The peak current increased as the incubation time increased and then remained constant after 60 min. Thus, 60 min was used as the optimal incubation time for the immunoassay (Fig. S5C). Fig. S5D shows that the peak current increased at pH less than 7.5 and decreased at pH greater than 7.5; therefore, pH 7.5 was used in the following experiments.

3.6. Analytical performance and reliability of the immunosensor

The analytical performance of this immunosensor was tested by SWV. In this experiment, 5 mM H_2O_2 was added to the electrolyte for signal amplification. The current response of the immunosensor increased with the increasing concentration of CYFRA21-1 (Fig. 4A). The immunosensor displayed good linear relation ranging from 0.1 pg mL^{-1} to 100 ng mL^{-1} with a low detection limit of 0.65 pg mL^{-1} (S/N = 3) (Fig. 4B). To investigate the reliability and accuracy of the above linear relationship, 14 serum samples containing CYFRA21-1 were analysed, and the obtained results were compared with electrochemiluminescence immunoassay (ECLI) tests (Table 1). Table 1 showed that the relative standard error was less than 10%, indicating good reliability of the immunosensor. To further verify the accuracy of the proposed biosensor in clinical application, 8 clinical serum samples containing CYFRA21-1 were analysed. The obtained results were compared with the standard addition method tests, and the relative standard error was determined to be less than 10%, indicating good reliability of the biosensor (Table S2).

Table 1
Assay results of clinical serum samples using the proposed immunosensor and ECLI.

Sample	Proposed immunosensor (ng mL^{-1})	ECLI (ng mL^{-1})	Relative error (%)
1	2.32	2.14	8.41
2	1.52	1.42	7.04
3	2.00	1.83	9.29
4	1.41	1.32	6.82
5	0.70	0.75	−6.66
6	1.13	1.06	6.60
7	2.24	2.15	4.19
8	1.52	1.40	8.57
9	0.50	0.47	6.38
10	0.62	0.58	6.90
11	1.50	1.60	−6.25
12	2.20	2.25	−2.22
13	1.29	1.38	−6.52
14	0.57	0.63	−9.52

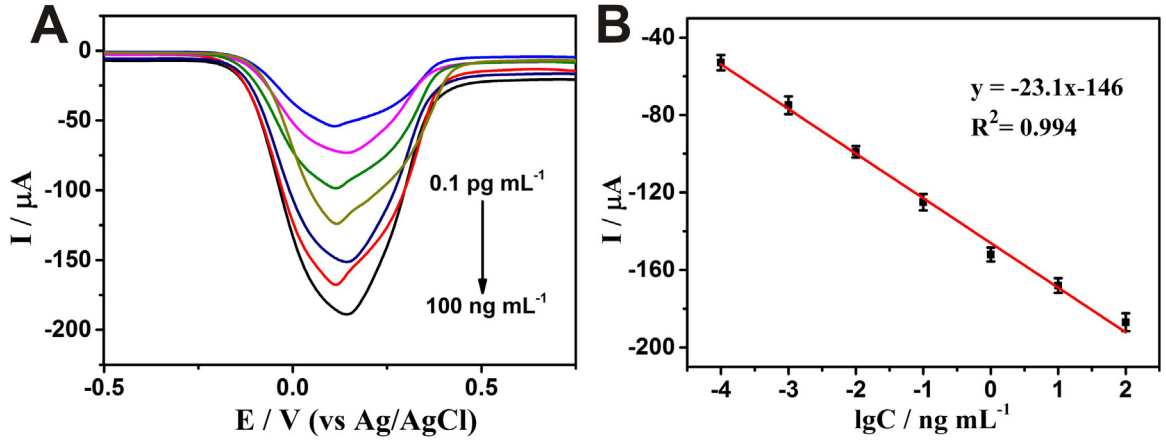

Fig. 4. SWV responses of electrochemical immunoassay in 0.01 M phosphate buffered solution, curves a–i correspond to CUFRA21-1 at the concentrations from 0.1 pg mL^{-1} to 100 ng mL^{-1} (A). The calibration plot between the SWV peak current and the logarithm values of MMP-2 concentrations (n = 3) (B).

3.7. Evaluation of selectivity, reproducibility, and stability of the immunosensor

To test the selectivity of this immunoassay, a mixture of UA, AA, CEA, AFP, PSA, and MMP-7 were used as the analyte instead of CYFRA21-1. Compared to the blank test (no target molecule) under the same testing conditions, no obvious change in the current was observed when the immunosensor was incubated with UA (1 ng mL^{-1}), AA (1 ng mL^{-1}), CEA (1 ng mL^{-1}), AFP (1 1 ng mL^{-1}), PSA (1 ng mL^{-1}), and MMP-7 (1 ng mL^{-1}). When CYFRA21-1 existed with the interferences, the electrochemical responses of samples containing CYFRA21-1 were almost the same regardless of the presence or absence of interferences (Fig. S6). All of these results indicate that the proposed immunosensor has good specificity for CYFRA21-1. To test the reproducibility of the immunosensor, three electrodes were prepared for the detection of 0.5 ng mL^{-1} CYFRA21-1. The relative standard error of the three electrodes was about 8%, suggesting good reproducibility of the proposed immunosensor. Furthermore, the immunosensor was stored at 4 °C for about 4 weeks to examine the stability, after which its electrochemical property was measured. The change in current response was less than 10%, revealing good stability of the immunoassay. Compared with previous reports, our proposed biosensor with the impedance-enhancer exhibits a wider detection range and higher sensitivity (Table S3).

4. Conclusion

In summary, a novel ZIF-8-HQ-BSA immunosensor probe was synthesised for the ultrasensitive detection of CYFRA21-1. By taking advantage of the components of the probe, an “off-on” strategy was applied in the immunosensor to amplify sensitivity. The immunosensing platform implementing this strategy exhibited a wide liner range and high sensitivity. This proposed method was further used to analyse CYFRA21-1 in human serum and demonstrated good consistency with an electrochemiluminescence immunoassay. To further improve this biosensor for practical application, the stepwise modification process on the electrode and detection process can be simplified. By conducting the modification process in a kit or tube, the analytical process can occur more effectively on the electrode to achieve better detection results. Overall, this proposed electrochemical immunosensor offers an advancement for further research on immunosensors for biomarker detection and their future industrial application.

CRediT authorship contribution statement

Huiqiang Wang: Investigation, Writing - original draft. **Zhanfang Ma:** Funding acquisition, Project administration, Supervision.

Acknowledgments

This research was financed by grants from the National Natural Science Foundation of China (21673143, 21273153), Natural Science Foundation of Beijing Municipality (2172016, 2132008), High-level Teachers in Beijing Municipal Universities in the Period of 13th Five-year Plan (IDHT20180517) and Capacity Building for Sci-Tech Innovation - Fundamental Scientific Research Funds (025185305000/195).

Declaration of interest statement

The authors declare no conflict of interest.

Appendix A. Supporting information

Supplementary data associated with this article can be found in the online version at doi:10.1016/j.bios.2019.03.013.

References

Cheng, H.J., Zhang, L., He, J., Guo, W.J., Zhou, Z.Y., Zhang, X.J., Nie, S.M., Wei, H., 2016. Anal. Chem. 88, 5489–5497.
Danielle, W.K., Gabriel, L., Mika, E.M., David, E.C., 2012. Anal. Chem. 84, 685–707.
Fan, H.X., 2015. Biosens. Bioelectron. 64, 51–54.
Karimi-Maleh, H., Biparva, P., Hatami, M., 2013. Biosens. Bioelectron. 48, 270–275.
Liang, Y.R., Zhang, Z.M., Liu, Z.J., Wang, K., Wu, X.Y., Zeng, K., Meng, H., Zhang, Z., 2017. Biosens. Bioelectron. 91, 199–202.
Liu, N., Chen, X., Ma, Z.F., 2013. Biosens. Bioelectron. 48, 33–38.
Liu, W.Y., Yang, H.M., Ma, C., Ding, Y.N., Ge, S.G., Yu, J.H., Yan, M., 2014. Anal. Chim. Acta 852, 181–188.
Lyu, F.J., Zhang, Y.F., Zare, R.N., Ge, J., Liu, Z., 2014. Nano Lett. 14, 5761–5765.
Moradi, R., Sebt, S.A., Karimi-Maleh, H., Sadeghi, R., Karimi, F., Bahari, A., Arabi, H., 2013. Phys. Chem. Chem. Phys. 15, 5888–5897.
Sanati, A.L., Karimi-Maleh, H., Badiei, A., Biparva, P., Ensafi, A.A., 2014. Mater. Sci. Eng. C. 35, 379–385.
Shan, J., Ma, Z.F., 2016. Microchim Acta 183, 2889–2897.
Tang, J., Huang, Y., Zhang, C., Liu, H.Q., Tang, D.P., 2016. Biosens. Bioelectron. 86, 386–392.
Tang, Z.X., Fu, Y.Y., Ma, Z.F., 2017a. Biosens. Bioelectron. 91, 299–305.
Tang, Z.X., Fu, Y.Y., Ma, Z.F., 2017b. Biosens. Bioelectron. 94, 394–399.
Wang, C.Q., Du, J., Wang, H.W., Zou, C., Jiang, F.X., Yang, P., Du, Y.K., 2014a. Sens. Actuators B 204, 302–309.
Wang, H.Q., Han, H.L., Ma, Z.F., 2017. Bioelectrochemistry 114, 48–53.
Wang, H.Q., Ma, Z.F., 2017. Microchim Acta 184, 1045–1050.
Wang, M.J., Sun, C.Y., Wang, L.Y., Ji, X.H., Bai, Y.B., Li, T.J., Li, J.H., 2003. J. Pharm. Biomed. 33, 1117–1125.
Wang, Y., Zhang, S., Du, D., Shao, Y.Y., Li, Z.H., Wang, J., Engelhard, M.H., Li, J.H., Lin, Y.H., 2011. J. Mater. Chem. 21, 5319.
Wang, Z.F., Liu, N., Ma, Z.F., 2014b. Biosens. Bioelectron. 53, 324–329.
Wang, Z.P., Hu, J.Q., Jin, Y., Yao, X., Li, J.H., 2006. Clin. Chem. 52, 1958–1961.
Wilson, M.S., 2005. Anal. Chem. 77, 1496–1502.
Xia, L., Wei, Z.X., Wan, M.X., 2010. J. Colloid Interface Sci. 341, 1–11.
Yang, Z.H., Chai, Y.Q., Yuan, R., Zhuo, Y., Li, Y., Han, J., Liao, N., 2014. Sens. Actuators B 193, 461–466.
Zheng, H.Q., Zhang, Y.N., Liu, L.F., Wan, W., Guo, P., Nystro¨m, A.M., Zou, X.D., 2016. J. Am. Chem. Soc. 138, 962–968.
Zou, C., Yang, B.B., Duan, B., Wang, J., Li, S.M., Yang, P., Wang, C.Q., Shiraishi, Y.K., Du, Y.K., 2017. J. Colloid Interface Sci. 488, 135–141.